

## Microscopic model analyses of the elastic scattering of 65 MeV protons from targets of diverse mass

P. J. Dortmans and K. Amos

*School of Physics, University of Melbourne, Parkville 3052, Victoria, Australia*

S. Karataglidis

*TRIUMF, 4004 Wesbrook Mall, Vancouver, British Columbia, Canada V6T 2A3*

J. Raynal

*C.E.A.-Saclay, Service de Physique Théorique, F-91191 Gif-sur-Yvette Cedex, France*

(Received 21 May 1998)

Nonlocal coordinate space optical potentials for the scattering of 65 MeV protons from nuclei ranging in mass from  ${}^6\text{Li}$  to  ${}^{238}\text{U}$  have been defined by folding a complex, medium-dependent effective interaction with the density matrix elements of each target. The effective interaction is based upon solutions of the Lippmann-Schwinger and Brueckner-Bethe-Goldstone equations having the Paris potential as input. The nuclear structure information required in our folding model is the one-body density matrix elements for the target and the single-nucleon bound state wave functions that they weight. For light mass nuclei, very large basis shell model calculations have been made to obtain the one-body density matrix elements. For medium and heavy mass nuclei, a very simple shell model prescription has been used. The bound-state single-particle wave functions that complete the nuclear density matrices are either Woods-Saxon or harmonic oscillator functions. The former are employed in most cases when large basis structure is available. For light nuclei ( $A \leq 16$ ) Woods-Saxon potential parameters and harmonic oscillator lengths are determined from fits to electron scattering form factors. For all other nuclei, we use harmonic oscillator functions with the oscillator lengths set from an  $A^{1/6}$  mass law. Using this microscopic model, optical potentials result from which differential cross sections, analyzing powers, and spin rotations are found. In general the calculated results compare very well with data when the effective interactions are determined from a mapping of nucleon-nucleon  $g$  matrices. This is not the case when effective interactions built from a mapping of (free)  $t$  matrices are used. [S0556-2813(98)05610-6]

PACS number(s): 25.40.Cm, 24.10.Ht

### I. INTRODUCTION

A microscopic, coordinate space model to analyze proton scattering from nuclei has been developed [1,2] from that formed earlier by the Hamburg group [3]. With this model, analyses have been made of 200 MeV proton elastic scattering from a large number of nuclei [4], of elastic and inelastic  $p$ - ${}^{12}\text{C}$  scattering over a range of incident energies [5], of charge exchange reactions [6], of the structure of neutron-rich nuclei such as  ${}^6,8\text{He}$  [7] and  ${}^9,11\text{Li}$  [8], and, very recently, of proton scattering from  ${}^3,4\text{He}$  [9]. Those light mass systems usually have been considered as few-body problems and the data analyzed with few-body methods. We note also that microscopic model analyses determined within a momentum space framework for elastic proton scattering have been made, with varying degrees of success [10–13]. The energies considered by these microscopic analyses (both in coordinate and momentum space) lie in a “transition” region between low and intermediate energies. For such energies, effects of nonlocalities in the effective nucleon-nucleus ( $NA$ ) interaction must be taken into account. Also for these energies, medium-dependent effects in the nucleon-nucleon ( $NN$ ) effective interaction, upon which that  $NA$  interaction is built, are important. When these two facets are taken into account in our coordinate space approach, good to excellent agreement with data is found to measured elastic and inelas-

tic scattering cross sections, analyzing powers, and other spin measureables [4,11]. The optical potentials are formed by folding the complex effective interaction with nuclear one-body density matrix elements (OBDME's) and a set of single-particle (SP) bound-state functions. For very light nuclei, modern shell model studies [14] not only specify the OBDME's but also which SP wave functions should be used. Using this information, calculations of both electron scattering form factors and proton elastic scattering observables become predictive, the latter especially when the effective interaction and folding procedure are fixed. Otherwise, one can use fits to the longitudinal elastic electron scattering form factor to specify the SP wave functions one should use in the  $NA$  scattering calculations. Those  $NA$  calculations then remain predictive as there is no adjustable quantity left. For heavier nuclei ( $A > 16$ ), shell model calculations to date have been made only within  $0\hbar\omega$  space. Therefore we have not used electron scattering form factor analyses to select a definitive set of SP wave functions. However, experience suggests [4] that harmonic oscillator (HO) functions with oscillator lengths following a simple mass rule ( $b = A^{1/6}$ ) should suffice.

Whatever the choice of structure input, the folding process leads to  $NA$  optical potentials that are nonlocal because of exchange (antisymmetry) contributions. In our model, antisymmetrization of the proton-target system has been taken

at the two-body level only; i.e., we have used a fully antisymmetrized  $A$ -nucleon target wave function and antisymmetrized each projectile-target nucleon pair. In the past, the resultant nonlocality of the optical potential either was ignored or was approximated by an equivalent local form [3]. Our calculations of 200 MeV proton-nucleus ( $pA$ ) scattering gave excellent predictions of observables but only when the complete integro-differential forms of Schrödinger equations were used [4].

As with our study at 200 MeV, we consider herein only the elastic scattering channel but take the spin rotation  $R$  into account along with the cross sections  $d\sigma/d\Omega$  and analyzing powers  $A_y$ . Specifically we have considered 50 targets, namely, the  $0p$ -shell nuclei  ${}^6,7,9,11\text{Li}$ ,  ${}^{11}\text{B}$ ,  ${}^{12}\text{C}$ , and  ${}^{16}\text{O}$ ; the  $1s0d$ -shell nuclei  ${}^{20}\text{Ne}$ ,  ${}^{24}\text{Mg}$ ,  ${}^{28}\text{Si}$ , and  ${}^{32}\text{S}$ ; the  $1s0d$  proton- $0f1p$  neutron shell nucleus,  ${}^{40}\text{Ar}$ ; the  $0f0p$ -shell  ${}^{40,42,44,48}\text{Ca}$ ,  ${}^{46,48,50}\text{Ti}$ ,  ${}^{52}\text{Cr}$ ,  ${}^{54,56}\text{Fe}$ ,  ${}^{59}\text{Co}$ , and  ${}^{58,60,62,64}\text{Ni}$ ; the  $2s1d0g$  neutron shell nuclei  ${}^{89}\text{Y}$ ,  ${}^{90}\text{Zr}$ ,  ${}^{98,100}\text{Mo}$ , and  ${}^{118}\text{Sn}$ ; the lanthanide nuclei,  ${}^{144,152,154}\text{Sm}$ ,  ${}^{160}\text{Gd}$ ,  ${}^{164}\text{Dy}$ ,  ${}^{166,168}\text{Er}$ , and  ${}^{174,176}\text{Yb}$ ; the  $0h_{11/2}$  proton- $0i_{13/2}$  neutron shell nuclei  ${}^{178,180}\text{Hf}$ ,  ${}^{182,184}\text{W}$ , and  ${}^{192}\text{Os}$ ; the mass 200 nuclei  ${}^{208}\text{Pb}$  and  ${}^{209}\text{Bi}$ ; and the actinide pair  ${}^{232}\text{Th}$  and  ${}^{238}\text{U}$ . Our predictions of elastic scattering from these diverse mass targets are compared with 65 MeV data in all cases with the exception of  ${}^9\text{Li}$ , the experimental data for which come from the elastic scattering of radioactive beams of those lithium isotopes from hydrogen. Inverse kinematics makes those experiments equivalent to 60 and 62 MeV protons scattering from  ${}^9\text{Li}$  and  ${}^{11}\text{Li}$ , respectively.

We compare predictions obtained from the optical potentials defined for each target with the proton elastic scattering data that are available, but only to  $80^\circ$  in the center of mass. In general, the cross-section magnitudes by that scattering angle are typically  $\sim 1$  mb/sr. We do not expect the approximations needed to make our model practical would be appropriate necessarily in making a prediction of the scattering of lesser magnitude.

The paper is arranged as follows. The procedure for obtaining our microscopic optical potentials is outlined in Sec. II, as are the amplitudes by which we obtain the proton scattering observables. In Sec. III we present and discuss the results for the scattering of 65 MeV protons from those nuclei included in the present study. Conclusions are drawn in Sec. IV.

## II. MICROSCOPIC OPTICAL POTENTIAL

We develop first the folding procedure by which the nonlocal optical potentials are specified. From those, the effective  $NA$  interaction is obtained and we define the amplitudes that specify the scattering observables.

### A. Folding process

In a representation with  $\mathbf{r}, \mathbf{r}'$  denoting relative coordinates between a colliding pair of particles, the Schrödinger equation describing their scattering by a local Coulomb,  $V_C(r)$ , plus a nonlocal hadronic (optical) potential takes the form

$$\left[ \frac{\hbar^2}{2\mu} \nabla^2 - V_C(r) + E \right] \Psi(\mathbf{r}) = \int U(\mathbf{r}, \mathbf{r}') \Psi(\mathbf{r}') d\mathbf{r}'. \quad (1)$$

This reduces, by using the partial wave expansions

$$\Psi(\mathbf{r}) = \sum_{lm} \frac{u_l(r)}{r} i^l Y_{lm}(\Omega_r) \quad (2)$$

and

$$U(\mathbf{r}, \mathbf{r}') = \sum_{lm} \frac{W_l(r, r')}{rr'} i^l Y_{lm}(\Omega_r) i^{-l} Y_{lm}^*(\Omega_{r'}), \quad (3)$$

to a set of integro-differential equations

$$\left\{ \frac{\hbar^2}{2\mu} \left[ \frac{d^2}{dr^2} - \frac{l(l+1)}{r^2} \right] - V_C(r) + E \right\} u_l(r) = \int_0^\infty W_l(r, r') u_l(r') dr'. \quad (4)$$

The  $W_l(r, r')$  contain both the local interaction and multipoles of the nonlocal interaction. Note that, for simplicity, we have suppressed all terms due to the intrinsic spin of the system. We seek solutions for  $NA$  scattering and determine the nonlocal interactions  $U_{NA}(\mathbf{r}, \mathbf{r}')$ , at 65 MeV in particular, by folding effective  $NA$  interactions with the relevant structure information. Thus we obtain the appropriate  $NA$  effective interaction for each nucleus in our investigation from  ${}^6\text{Li}$  to  ${}^{238}\text{U}$ . At this particular energy one may anticipate stronger influences in analyses of the medium effects defining the effective  $NN$  interactions and of the nonlocalities in the optical potentials arising from the folding process than in studies of 200 MeV scattering [4]. With the optical potential in this coordinate space representation, we use the program DWBA91 [15] to solve the set of partial wave integro-differential Schrödinger equations. That code has the further useful attribute that it can be used to evaluate distorted wave Born approximated (DWBA) amplitudes for inelastic scattering, given the appropriate OBDME and SP wave functions. The microscopic optical potentials are used therein to determine the distorted waves and the medium modified effective  $NN$  interaction is used as the transition operator. Data from inelastic scattering of 200 MeV protons from  ${}^6,7\text{Li}$  and  ${}^{12}\text{C}$  have been well reproduced by using that procedure [2,16], further justifying the scattering theory formulated in coordinate space.

To define the nonlocal interaction for  $NA$  scattering in a full folding model, we must accommodate antisymmetry between the projectile and every nucleon specified with the internal nuclear wave function. We must evaluate multiparticle matrix elements of the form

$$U_{pA} = \left\langle \Psi(1, \dots, A) \left| \sum_{N=1}^A V_{N0} \right| \Psi(1, \dots, A) \right\rangle, \quad (5)$$

with  $\langle \mathbf{R} | \Psi(1, \dots, A) \rangle$  being the many-body wave function for the ground state of the target and “0” denoting the projectile coordinates. As all nucleons in the target are equivalent, it is useful to choose a specific entry (“1”) and write

$$U_{pA} = A \langle \Psi(1, \dots, A) | V_{10} | \Psi(1, \dots, A) \rangle. \quad (6)$$

With the many-body state expanded in cofactors,

$$|\Psi(1, \dots, A)\rangle = \frac{1}{\sqrt{A}} \sum_{\alpha m} |\varphi_{\alpha m}(1)\rangle a_{\alpha m} |\Psi(1, \dots, A)\rangle, \quad (7)$$

where  $\alpha$  specifies the set  $\{n, l, j, \zeta\}$  and  $\zeta$  is the isospin projection, Eq. (6) becomes

$$U_{pA} = \sum_{\alpha m \alpha' m'} \langle \Psi | a_{\alpha' m'}^\dagger a_{\alpha m} | \Psi \rangle \times \langle \varphi_{\alpha' m'}(1) | V_{10} \{ |\varphi_{\alpha m}(1)\rangle - |\varphi_{\alpha m}(0)\rangle \}, \quad (8)$$

when the required antisymmetry with projectile and struck nucleon is taken into account. The nuclear structure information required to evaluate the optical potentials is many-body matrix elements of the particle-hole operators. They are defined by

$$\rho_{\alpha \alpha' J_i J_f}^{m m' M_i M_f} = \langle \Psi | a_{\alpha' m'}^\dagger a_{\alpha m} | \Psi \rangle = \sum_{I, N} \frac{(-1)^{j-m}}{\sqrt{2J_f+1}} \times \langle j m j' - m' | I - N \rangle \langle J_i M_i I N | J_f M_f \rangle S_{\alpha \alpha' I}, \quad (9)$$

where the OBDME's  $S_{\alpha \alpha' I}$  are [with  $\tilde{a}_{\alpha m} = (-1)^{j-m} a_{\alpha -m}$ ]

$$S_{\alpha \alpha' I} = \langle \Psi_{J_f} | [a_{\alpha'}^\dagger \times \tilde{a}_{\alpha}]^I | \Psi_{J_i} \rangle \rightarrow \langle \Psi_J | [a_{\alpha'}^\dagger \times \tilde{a}_{\alpha}]^I | \Psi_J \rangle, \quad (10)$$

in the elastic scattering case (from a target with spin  $J$ ). If  $J$  is nonzero, multipoles from 0 to  $I_{\max}(=2J)$  contribute. Scattering from light odd mass targets show that these must be included [16]. As even-even nuclei all have ground state spin parities ( $J^\pi$ ) of  $0^+$ , the required OBDME's simply are the monopoles

$$S_{\alpha \alpha' 0} = \langle \Psi_0 | [a_{\alpha'}^\dagger \times \tilde{a}_{\alpha}]^0 | \Psi_0 \rangle. \quad (11)$$

While the angular momentum selection rules require  $l=l'$  and  $j=j'$ , there is no such restriction on the principle quantum number. The cases where  $n \neq n'$  signify purely radial excitations which can only occur in spaces allowing for cross shell transitions. In those instances, the specification of the full density requires the inclusion of those off-diagonal elements. The diagonal elements reduce to the shell occupancies as

$$\langle \Psi | a_{\alpha' m'}^\dagger a_{\alpha m} | \Psi \rangle \rightarrow \delta_{\alpha \alpha'} \delta_{m m'} \sigma_{\alpha \alpha'}, \quad (12)$$

where  $\sigma_{\alpha \alpha}$  is the fractional shell occupancy as a fully occupied shell has  $\sigma_{\alpha \alpha} = 1$ . Thus the (diagonal) OBDME's are given by

$$S_{\alpha \alpha 0} = \sqrt{2j+1} \sigma_{\alpha \alpha}. \quad (13)$$

The optical potential given by this folding process takes the form

$$U(\mathbf{r}_1, \mathbf{r}_2; E) = \sum_{\alpha m \alpha' m'} (2j+1) \sigma_{\alpha \alpha'} \times \left[ \delta(\mathbf{r}_1 - \mathbf{r}_2) \int \varphi_{\alpha' m'}^*(\mathbf{s}) U^D(R_{1s}, E) \varphi_{\alpha m}(\mathbf{s}) d\mathbf{s} + \varphi_{\alpha' m'}^*(\mathbf{r}_1) U^{Ex}(R_{12}, E) \varphi_{\alpha m}(\mathbf{r}_2) \right], \quad (14)$$

where  $R_{12} = |\mathbf{r}_1 - \mathbf{r}_2|$ , and  $U^D$  and  $U^{Ex}$  are appropriate combinations of the multipoles of the effective interaction for the direct and exchange contributions to the optical potential respectively [3,15]. One then applies the partial wave expansions, Eq. (3).

A feature in our process of analysis is that all details required to make the calculations are preset. In the cases of  ${}^6,7\text{Li}$  [16] and of  ${}^{12}\text{C}$  [2], nuclear structure information was taken from shell model calculations in complete multi- $\hbar\omega$  spaces with the SP wave functions set by fits to the longitudinal elastic electron scattering form factors. Thus the results for both the elastic and inelastic scattering of 200 MeV protons from those nuclei were obtained from single calculations. No adjustments (such as those attributed to core polarizations) were needed and most proton excitation data were well described. With the microscopic (coordinate space) model for 200 MeV  $pA$  scattering established for a set of  $0p$ -shell nuclei, an extensive analysis for many more nuclei with masses up to  ${}^{208}\text{Pb}$  was completed [4]. In almost all cases single calculations led to excellent reproduction of data. Most recently [9], wave functions from very large space shell model calculations of  ${}^3\text{He}$  were used in successful predictions of the elastic scattering of 200 MeV protons from that few-nucleon system. In that case the shell model interaction used also fixed the SP wave functions, and so the analysis of the electron scattering form factor was also predictive.

## B. Effective interaction

The folding procedure to define the optical potential requires the specification of the  $NN$  effective interaction in  $ST$ -channel form and in coordinate space. This effective interaction we take as a mixture of central, two-body spin-orbit and tensor force attributes, each having a form factor that is a set of four Yukawa functions with complex coefficients, i.e.,

$$g_{eff}^{(i)ST}(r, E) = \sum_{k=1}^{n_i} S_k^{(i)}[\rho(r), E] \frac{e^{-(\mu_k^{(i)} r)}}{r}. \quad (15)$$

Therein  $S_k^{(i)}[\rho(r), E]$  are complex strengths that vary with projectile energy and nuclear density;  $\mu_k^{(i)}$  are the inverse ranges of the Yukawa functions with  $k$  the index for those inverse ranges. In principle, the number of strengths and inverse ranges ( $n_i$ ) chosen can be as large as one likes, though for all operators  $n_i=4$  seems to be sufficient to reproduce accurately the half-off-shell  $g$  matrices for laboratory energies between 50 and 400 MeV [1]. Singular-valued decom-

position was used to optimize those inverse ranges and coefficients so that double Bessel transforms of the effective interaction map accurately to an appropriate set of infinite nuclear matter  $g$  matrices [17,18] obtained from solution of the Bethe-Brueckner-Goldstone (BBG) equation,

$$g_{LL'}^{(JST)}(p', p; k, K, k_F) = V_{LL'}^{(JST)}(p, p') + \frac{2}{\pi} \sum_I \int_0^\infty V_{LI}^{(JST)}(p', q) [\mathcal{H}] \times g_{LL'}^{(JST)}(q, p; k, K, k_F) q^2 dq, \quad (16)$$

where

$$\mathcal{H}(q, k, K, k_f) = \frac{\bar{Q}(q, K, k_f)}{\bar{E}(k, K, k_f) - \bar{E}(q, K, k_f) + i\varepsilon}, \quad (17)$$

in which  $\bar{Q}(q, K, k_f)$  is an angle-averaged Pauli operator with an average center-of-mass momentum  $K$  [17,18]. The energies in the propagators of the BBG equations include auxiliary potentials  $U$  and are defined by

$$\bar{E}(q, K, k_f) = (q^2 + K^2) + \left(\frac{m}{\hbar^2}\right) \{U(|\mathbf{q} + \mathbf{K}|) + U(|\mathbf{q} - \mathbf{K}|)\}, \quad (18)$$

wherein  $U$  is the first-order mass operator term. We take  $V_{LL'}^{(JST)}(p, p')$  to be the Paris  $NN$  interaction [19], although there is little difference if one starts with the Bonn  $NN$  potential [2]. Details of the techniques involved are given elsewhere [17,18].

Given that the  $NN$   $g$  matrices are most easily specified in momentum space and the effective interaction form is an approximation, it is sensible to seek to analyze  $NA$  elastic scattering with a momentum space solution of the Schrödinger equation. Such studies have been made using credible  $g$  matrices as input [11,12] and those results reflect reasonable agreement with the data. They also confirm the need for inclusion of medium effects for low and intermediate energy  $NA$  scattering. Of note from the momentum space calculations is the observation that off-shell Kowalski-Noyes  $f$  ratios of the  $t$  and  $g$  matrices vary quite similarly [18]. The major effect of medium modifications (Pauli blocking and energy denominators) is to vary the on-shell values.

The choice of the Yukawa forms for the effective interaction is extremely advantageous when it comes to evaluating the optical potential. Fourier transformation of each of the radial components of the effective  $NN$  interactions gives a simple multipole form, so that for the central terms, the double Bessel transformation that leads to each term in the nonlocal interaction can be solved analytically, taking the form

$$W_i^{(k)}(r_1, r_2) \propto h_i^{(+)}(i\mu^{(k)} r_>) j_i(i\mu^{(k)} r_<), \quad (19)$$

where  $r_<$  and  $r_>$  are the lesser and greater of  $r_1$  and  $r_2$ , respectively.

### C. Observables

There are diverse observables for the scattering of polarized protons from an unpolarized target. While one may define differing sets, we consider that which involves the differential cross section  $d\sigma/d\Omega$ , analyzing power  $A_y$ , and two Wolfenstein spin rotations  $A$  and  $R$ . These measurable are defined in terms of scattering amplitudes  $F(\theta)$  [20]. Since the data we investigate were obtained using polarized projectile protons, this amplitude is a  $2 \times 2$  matrix,

$$F(\theta) = \begin{vmatrix} f_{1/2 \ 1/2}(\theta) & f_{1/2-1/2}(\theta) \\ -f_{1/2-1/2}(\theta) & f_{1/2 \ 1/2}(\theta) \end{vmatrix}, \quad (20)$$

where

$$f_{1/2 \ 1/2}(\theta) = f_C(\theta) r_{1/2 \ 1/2}^{(1/2)}(\theta) + \frac{1}{4ik} \sum_J (2J+1) e^{-2i\sigma_J^C} \times (S_J^+ + S_J^- - 2) r_{1/2 \ 1/2}^{(J)}(\theta), \quad (21)$$

and

$$f_{1/2-1/2}(\theta) = f_C(\theta) r_{1/2-1/2}^{(1/2)}(\theta) + \frac{1}{4ik} \sum_J (2J+1) e^{-2i\sigma_J^C} \times (S_J^+ - S_J^-) r_{1/2-1/2}^{(J)}(\theta). \quad (22)$$

Here  $r_{1/2\pm 1/2}^{(J)}(\theta)$  are the rotation matrices,  $\sigma_J^C$  are the Coulomb phase shifts,  $f_C(\theta)$  is the point Coulomb scattering amplitude, and  $S_J^\pm$  are the  $S$  matrices for  $J=L\pm\frac{1}{2}$ . With these, the elastic scattering observables are defined as

$$\frac{d\sigma}{d\Omega}(\theta) = |f_{1/2 \ 1/2}(\theta)|^2 + |f_{1/2-1/2}(\theta)|^2, \quad (23)$$

$$A_y(\theta) = P(\theta) = \frac{2 \operatorname{Im}\{f_{1/2 \ 1/2}(\theta) f_{1/2-1/2}^*(\theta)\}}{|f_{1/2 \ 1/2}(\theta)|^2 + |f_{1/2-1/2}(\theta)|^2}, \quad (24)$$

$$R(\theta) = K_x^x(\theta) = K_z^z(\theta) = \frac{|f_{1/2 \ 1/2}(\theta)|^2 - |f_{1/2-1/2}(\theta)|^2}{|f_{1/2 \ 1/2}(\theta)|^2 + |f_{1/2-1/2}(\theta)|^2}, \quad (25)$$

and

$$A(\theta) = K_z^x(\theta) = -K_x^z(\theta) = \frac{2 \operatorname{Re}\{f_{1/2 \ 1/2}(\theta) f_{1/2-1/2}^*(\theta)\}}{|f_{1/2 \ 1/2}(\theta)|^2 + |f_{1/2-1/2}(\theta)|^2}. \quad (26)$$

Commonly  $Q$ , a linear combination of the Wolfenstein spin rotations, is measured. It relates to the above by

$$Q(\theta) = R(\theta) \sin\theta + A(\theta) \cos\theta. \quad (27)$$

TABLE I. Table of calculated  $pA$  reaction cross sections (in mb) at 65 MeV.

Nucleus	$g$ folding	$t$ folding	Nucleus	$g$ folding	$t$ folding
${}^6\text{Li}$	234	303	${}^{60}\text{Ni}$	929	1084
${}^7\text{Li}$	274	343	${}^{62}\text{Ni}$	957	1110
${}^9\text{Li}$	288	388	${}^{64}\text{Ni}$	1011	1158
${}^{11}\text{Li}$	408	501	${}^{89}\text{Y}$	1221	1361
${}^{11}\text{B}$	310	410	${}^{90}\text{Zr}$	1224	1364
${}^{12}\text{C}$	304	411	${}^{98}\text{Mo}$	1318	1450
${}^{16}\text{O}$	366	486	${}^{100}\text{Mo}$	1343	1472
${}^{20}\text{Ne}$	450	576	${}^{118}\text{Sn}$	1467	1591
${}^{24}\text{Mg}$	482	619	${}^{144}\text{Sm}$	1655	1777
${}^{28}\text{Si}$	533	680	${}^{152}\text{Sm}$	1768	1881
${}^{32}\text{S}$	586	737	${}^{154}\text{Sm}$	1782	1893
${}^{40}\text{Ar}$	679	859	${}^{160}\text{Gd}$	1804	1918
${}^{40}\text{Ca}$	675	831	${}^{164}\text{Dy}$	1840	1947
${}^{42}\text{Ca}$	718	872	${}^{166}\text{Er}$	1834	1941
${}^{44}\text{Ca}$	757	909	${}^{168}\text{Er}$	1853	1958
${}^{48}\text{Ca}$	829	977	${}^{174}\text{Yb}$	1888	2007
${}^{46}\text{Ti}$	761	923	${}^{178}\text{Hf}$	1920	2022
${}^{48}\text{Ti}$	799	956	${}^{182}\text{W}$	1936	2043
${}^{50}\text{Ti}$	835	990	${}^{192}\text{Os}$	2019	2117
${}^{52}\text{Cr}$	843	999	${}^{197}\text{Au}$	2024	2110
${}^{54}\text{Fe}$	853	1011	${}^{208}\text{Pb}$	2102	2192
${}^{56}\text{Fe}$	888	1044	${}^{209}\text{Bi}$	2109	2196
${}^{59}\text{Co}$	924	1078	${}^{232}\text{Th}$	2262	2339
${}^{58}\text{Ni}$	895	1053	${}^{238}\text{U}$	2270	2346

III. RESULTS

In the following subsections, we display the results of our calculations of the elastic scattering of 65 MeV protons from many target nuclei and place them in comparison with experimental data wherever such data exist. The results are subdivided into four sections. First, we present the scattering from the light nuclei,  ${}^6\text{Li}$  to  ${}^{16}\text{O}$ , for which OBDME's have been obtained mostly from large space shell model calculations and for which SP wave functions have been determined from fits to the longitudinal elastic electron scattering form factors. Then we present and discuss the results obtained with medium mass nuclei, from  ${}^{20}\text{Ne}$  to  ${}^{64}\text{Ni}$ . For those nuclei the shell model calculations were performed in complete  $0\hbar\omega$  spaces, except for those in the middle of the  $fp$  shell where the dimension of the basis becomes prohibitively large for matrix diagonalization techniques. In those cases, a restriction on the number of nucleons in the  $0f_{7/2}$  orbit was placed on the model. The oscillator length for the HO SP wave functions used was set as  $A^{1/6}$  (in units of fm). In the third section, we present the results for the scattering from heavy nuclei, and in which the nucleon occupancies are those given by a simple packing model. Again we use HO wave functions with an oscillator length given by  $A^{1/6}$  fm as the SP functions. In the final section, we consider the changing structure of the observables across the mass range.

For each of the cases discussed, we present the results of

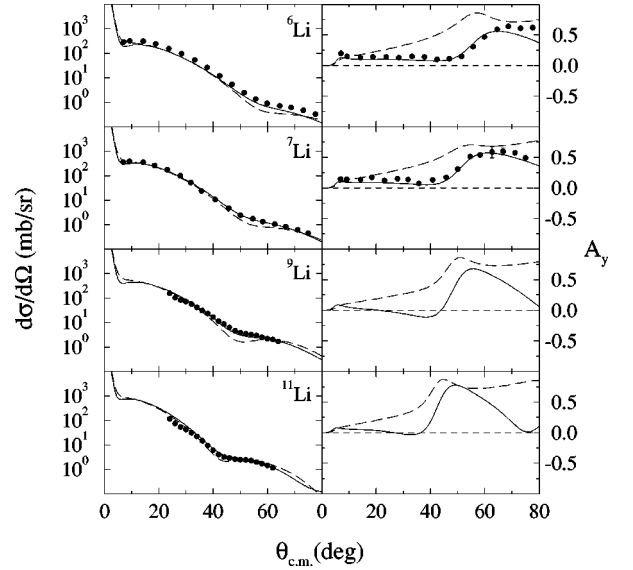


FIG. 1. The differential cross sections (left) and analyzing powers (right) from the elastic scattering of 65 MeV protons from  ${}^{6,7,9,11}\text{Li}$ . The data (dots) are compared with the results of our microscopic model calculations for the cases when medium effects are included (solid curves) or are ignored (dashed curves). Data were taken from Refs. [22,23].

two calculations. They differ only in the specification of the optical potential. The results obtained with the effective interaction built from the  $NN$   $g$  matrices folded with known density profiles [21] are displayed by the solid curves while those found using the free  $NN$   $t$  matrices are displayed by the dashed curves. For simplicity we designate the results as being obtained from calculations made using  $g$ -folding and  $t$ -folding potentials, respectively. The data come from Refs. [22–33] with specific reference made in the figure captions. For completeness, the total reaction cross sections obtained from our calculations made with the  $g$ -folding and  $t$ -folding models are presented in Table I. Clearly the effect of the nuclear medium is to reduce the expected total cross section. The cross sections increase in a consistent manner with mass for most nuclei. However, it is interesting to note that the result for  ${}^{11}\text{Li}$  is considerably larger than that for  ${}^{11}\text{B}$ . Although the  ${}^{11}\text{Li}$  calculation was made for 62 MeV (at which there is differential cross-section data) rather than 65 MeV, the energy variation is insufficient to explain the resulting 30% increase in the total cross section. Rather we attribute that substantial difference to the extended nature of the halo nucleus.

A. Light mass nuclei ( $A \leq 16$ )

The results of our calculations of the elastic scattering of 65 MeV protons from light mass nuclei are shown in Figs. 1 and 2. The differential cross sections  $d\sigma/d\Omega$  and analyzing powers  $A_y$  are displayed in the left and right panels, respectively. The target is identified in each segment of the diagrams. The ground state wave functions were obtained, for the most part, from shell model calculations made within a complete  $(0+2)\hbar\omega$  model space. The exceptions were  ${}^{6,7}\text{Li}$ , for which the wave functions were obtained in a complete  $(0+2+4)\hbar\omega$  space [16]. The SP wave functions were

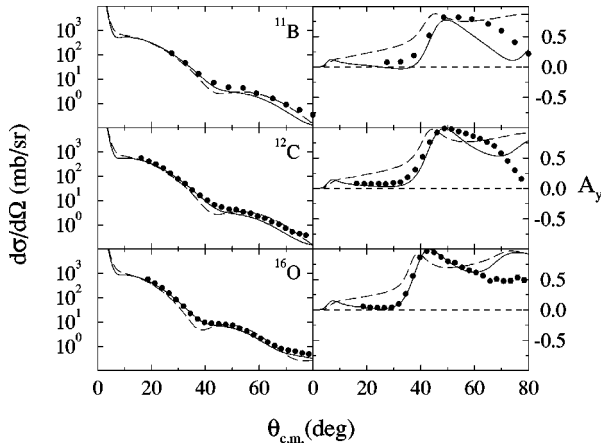


FIG. 2. As for Fig. 1 but for  $^{11}\text{B}$ ,  $^{12}\text{C}$ , and  $^{16}\text{O}$ . Data were taken from Refs. [24–27].

assumed to be of Woods-Saxon (WS) form and were chosen to reproduce the longitudinal elastic electron scattering form factor data. For  $^{16}\text{O}$ , HO functions were used.

The differential cross sections and analyzing powers for the elastic scattering of protons from four lithium isotopes are displayed in Fig. 1. In the case of  $^6\text{Li}$ , our prediction of the cross section made with the  $g$ -folding potential has the correct shape but it is slightly weaker than the data. This is not the case at 200 MeV [16], where the data are well reproduced. The slight discrepancy at the lower energy may be a consequence of the deformation of the target and the failure of the shell model, even in the  $(0+2+4)\hbar\omega$  space, to reproduce the cluster nature of the  $^6\text{Li}$  nucleus [16]. Yet, although  $^6\text{Li}$  does not have a large central density, the changes as a result of the medium modifications contained in the  $g$  matrix are quite significant. This is observed in comparison to the results obtained using the  $t$ -folding potential. The measured cross section is not reproduced as well with that result as with the  $g$ -folding one, although the discrepancies are not large. However, as noted previously [2,11,34], the analyzing powers are very sensitive to the details of the density in the folding. We find this to be the case again, and at 65 MeV, with all of the light nuclei. Our results of scattering from  $^7\text{Li}$  are better, as now our prediction for the cross section obtained using the  $g$ -folding potential is only marginally weaker than the data. The analyzing power is also well reproduced out to  $80^\circ$ .

For  $^9\text{Li}$ , the medium modification effects on the cross section are quite pronounced. In this case, it is essential to use the results from  $g$  folding. Currently there are no data for the spin observables or for form factors from electron scattering for the exotic nuclei so that the proton cross section represents the best available test of putative structures. In this case, as for  $^{11}\text{Li}$ , the density profile was obtained directly from the shell model ground state. Also, in the absence of any electron scattering data, we used WS SP wave functions appropriate for electron scattering from  $^9\text{Be}$ . With such a specification, the result obtained from the  $g$ -folding potential is remarkably good.

The final results shown in Fig. 1 are for  $^{11}\text{Li}$  as the target. This nucleus has a halo distribution associated with the very loosely bound valence neutron pair. To allow for this extension in the density we use WS SP wave functions with the

binding energy for the  $0p_{1/2}$  and higher shell neutrons set to 500 keV [8]. The WS functions assumed for the  $0s_{1/2}$  and  $0p_{3/2}$  orbits were those used for  $^9\text{Li}$ , consistent with the model for  $^{11}\text{Li}$  of a two-neutron halo outside a  $^9\text{Li}$  core. With that prescription, our prediction adequately reproduces the data, although it slightly overestimates the cross section at the small scattering angles. Even so, using such a simple model to describe the halo nature of this nucleus produces results that give us confidence to use proton scattering to study the matter distributions of other neutron and proton-rich nuclei.

We note in passing that for a target with nonzero spin it is essential to include all multipole contributions in the scattering, as is the case with all the lithium isotopes. In Eq. (10), there are  $2J+1$  possible multipoles in the specification of the ground state. The contributions of nonzero multipoles are not large, but they are important. The analyzing power is especially sensitive to them, as is most dramatically seen in the results for proton scattering from  $^9\text{Be}$  [4,35].

The results for scattering from  $^{11}\text{B}$ ,  $^{12}\text{C}$ , and  $^{16}\text{O}$  are presented in Fig. 2. For  $^{11}\text{B}$ , our predictions compare least favorably with the data, although the cross section and analyzing power still are well described out to  $40^\circ$ . Above this, the predicted cross section falls at a slightly greater rate than that indicated by the data. However, the effects of the medium modifications in the effective  $NV$  interaction are essential for any adequate description of the analyzing power. With the other nuclei, the  $g$ -folding model predictions are all very good. They are clearly better representations of the data, especially the analyzing powers, than are the results found with the  $t$ -folding model. Note that the range involves at least three orders of magnitude in the cross section.

## B. Medium mass nuclei ( $16 < A \leq 64$ )

While for light mass nuclei it is now possible to make shell model calculations using large and complete spaces, for  $1s0d$ - and  $0f1p$ -shell nuclei, such “no-core” determinations of the shell model wave functions as yet are not feasible. The size of the spaces necessary are prohibitively large. For a number of nuclei, however, it is still possible to construct complete  $0\hbar\omega$ -shell models for use in analyses of elastic scattering data. Those models still require core polarization corrections and hence the use of the density matrices in analyses of electron scattering data may not be as good a check on the SP wave functions as with the  $0p$ -shell nuclei. Therefore we have assumed HO functions with  $A^{1/6}$  fm for all subsequent calculations of the proton scattering observables for nuclei with  $A \geq 20$ .

The results for the elastic scattering of 65 MeV protons from  $^{20}\text{Ne}$ ,  $^{24}\text{Mg}$ ,  $^{28}\text{Si}$ , and  $^{32}\text{S}$  are presented in Fig. 3. A complete  $0\hbar\omega$ - ( $1s0d$ )- shell model calculation was performed for all nuclei. The results of our  $g$ -folding model calculations reproduce the cross-section data for the scattering from  $^{24}\text{Mg}$  and  $^{28}\text{Si}$  well and at all scattering angles to  $80^\circ$ . For  $^{20}\text{Ne}$ , the description is accurate to  $60^\circ$  at least. However, for scattering from  $^{32}\text{S}$ , the level of agreement with the cross-section data is less than satisfactory. Also, in all cases, the level of agreement between the results of our calculations using the  $t$ -folding model and the data is poorer. This poor reproduction we find from our  $g$ -folding model to

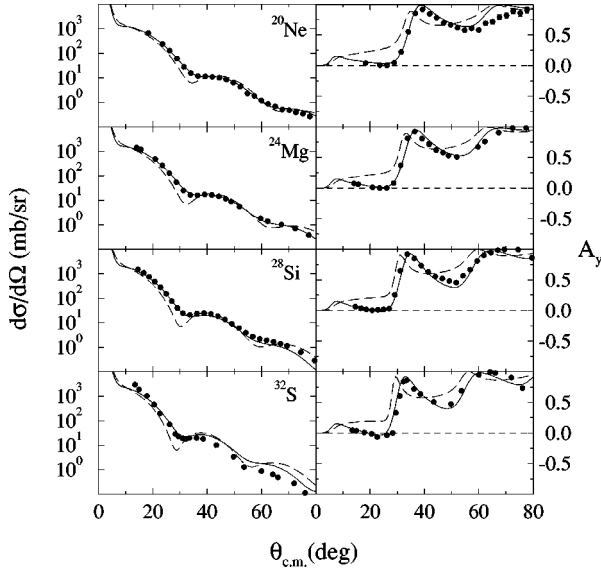


FIG. 3. As for Fig. 1 but for  $^{20}\text{Ne}$ ,  $^{24}\text{Mg}$ ,  $^{28}\text{Si}$ , and  $^{32}\text{S}$ . Data were taken from Refs. [26,27].

the  $^{32}\text{S}$  cross-section data cannot be due simply to the choice of oscillator length. The cross-section data for  $^{32}\text{S}$  have magnitudes considerably larger than those of  $^{28}\text{Si}$  (and of  $^{40}\text{Ar}$ , which we show next) for small scattering angles and vice versa for larger scattering angles. It is known that these  $1s0d$ -shell nuclei are deformed and that  $^{32}\text{S}$  is different from the others. That is evidenced by  $^{32}\text{S}$  not having the distinctive splitting of the giant dipole resonances that occur in  $^{24}\text{Mg}$  and  $^{28}\text{Si}$ . The different deformation of  $^{32}\text{S}$  might explain the difference we see in the quality of reproduction of the scattering data. Certainly when a phenomenological optical model analysis was used to fit the same scattering data, the parameters required to fit the  $^{32}\text{S}$  data were quite different from those found with data off the neighboring nuclei [26]. As with the results presented for the light nuclei, the differences between the results obtained using the  $g$ - and  $t$ -folding models are far more significant in the analyzing powers. In all cases, those results obtained with the  $g$ -folding models reproduce the data well. We also note that there is a definite trend in the size and shape of the data as one increases the mass of the target. The data indicate a sharp rise from 0 at  $0^\circ$  to a maximum near 1 followed by a fall and a second peak of similar character. The first peak becomes more forward peaked as the mass of the target increases ( $60^\circ$  for  $^6\text{Li}$ ,  $30^\circ$  for  $^{28}\text{Si}$ ). This could be used as an indicator for optimum SP wave functions, as small changes in the HO parameter produce shifts in the position of this peak in the analyzing power.

The results for the elastic scattering of 65 MeV protons from  $^{40}\text{Ar}$  and  $^{40}\text{Ca}$  are displayed in Fig. 4. The analyzing powers have small differences with the most notable being a small shift in the angles of structures. The differential cross sections also are different with the position and size of the prominent peak being the primary effect. For  $^{40}\text{Ar}$ , that feature occurs at  $33^\circ$  and has a value of 60 mb/sr. For  $^{40}\text{Ca}$ , the result is 44 mb/sr at  $36^\circ$ . For both these nuclei, a ‘packed’ model of their structure has been used in our analyses. Specifically  $^{40}\text{Ca}$  has been taken as a doubly closed shell nucleus

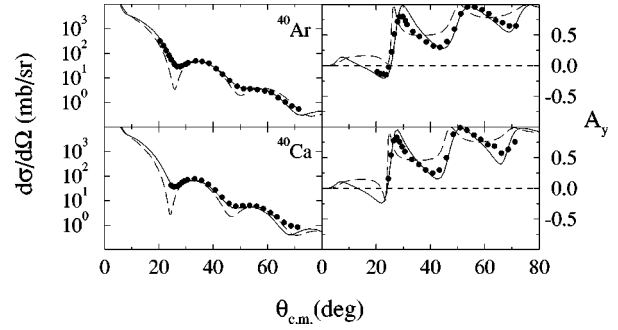


FIG. 4. As for Fig. 1 but for  $^{40}\text{Ar}$  and  $^{40}\text{Ca}$ . Data were taken from Refs. [26–28].

while  $^{40}\text{Ar}$  has been taken as two proton holes (in the  $d_{3/2}$  subshell) with two extra core nucleons (in the  $f_{7/2}$  orbit) on that doubly closed shell description. The agreement with data for the scattering from  $^{40}\text{Ar}$  is good to  $60^\circ$ . The differences between the Ar and Ca results are consistent with observed differences in the data sets and reflect the effects of surface contributions revealed by a change of basic structure from the closure of a major shell.

In the case of  $^{40}\text{Ca}$ , our  $t$ -folding model results are quite similar to those obtained recently in a momentum space framework [13], while our  $g$ -folding model results agree quantitatively with those found using a  $g$  matrix in another momentum space calculation [11]. These differences emphasize that one cannot neglect the importance of the medium in specifying the effective interaction, whether it is for scattering at 200 MeV [2] or at 65 MeV [34].

The results of our calculations using the  $g$ - and  $t$ -folding models are compared with data for the case of scattering from the heavier calcium isotopes in Fig. 5. As with the lighter nuclei, we again note that the results found using the optical potentials specified in the  $g$ -folding model are in excellent agreement with the data up to  $70^\circ$ . Again those results differ markedly from ones obtained using the optical potentials in the  $t$ -folding model. Also, the trend in the analyzing power noted earlier is observed in the calcium isotopes. However, there are more pronounced minima in the cross sections, and the analyzing powers show a new minimum developing at small scattering angles.

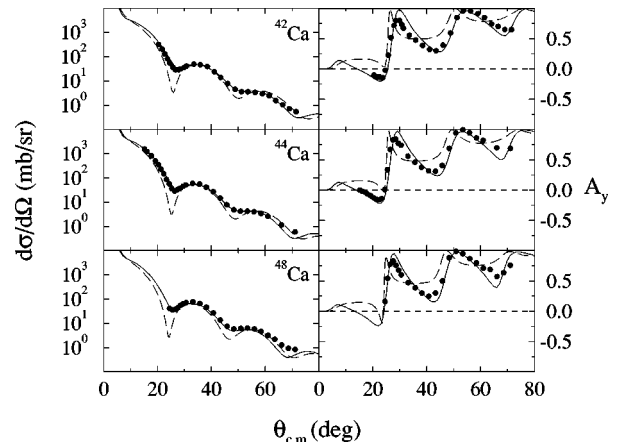


FIG. 5. As for Fig. 1 but for  $^{42,44,48}\text{Ca}$ . Data were taken from Refs. [27,28].

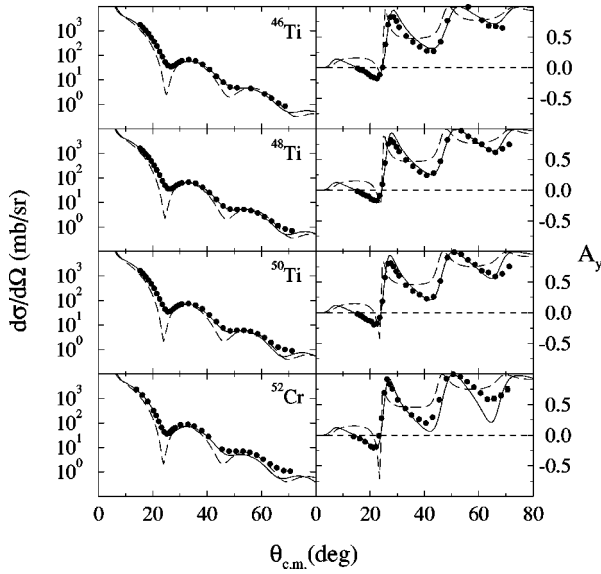


FIG. 6. As for Fig. 1 but for  $^{46,48,50}\text{Ti}$  and  $^{52}\text{Cr}$ . Data were taken from Refs. [27,28].

The results for the scattering from  $^{46,48,50}\text{Ti}$  and  $^{52}\text{Cr}$  are displayed in Fig. 6. The agreement between the data for the scattering of 65 MeV protons from the titanium isotopes and the results from our  $g$ -folding model calculations is quite good to  $70^\circ$ . That level of agreement is not observed in the case of scattering from  $^{52}\text{Cr}$ ; the data are underpredicted above  $45^\circ$ . However, the shape indicated by the data is by far better reproduced by the  $g$ -folding result than the  $t$ -folding one. This underprediction at large angles is observed in the scattering from  $^{54,56}\text{Fe}$  and  $^{59}\text{Co}$ , displayed in Fig. 7, and also in the scattering from the Ni isotopes, displayed in Fig. 8. In these cases, a complete  $0\hbar\omega$ -shell model calculation is not possible with the standard diagonalization techniques; those are only calculable in an approximate fashion using Monte Carlo techniques. For the present calculations, the model space in the shell model calculation was restricted to close the  $0f_{7/2}$  orbit. This could cause the observed discrepancy with the data. Also, the choice for the oscillator length might not be optimal. One could choose to set  $b$  by a best fit to the cross-section and analyzing power data, as we

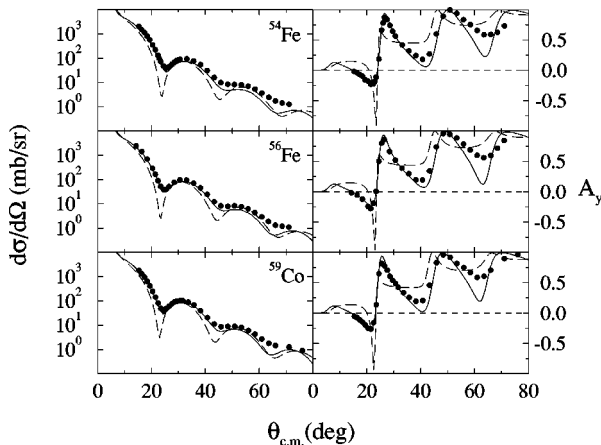


FIG. 7. As for Fig. 1 but for  $^{54,56}\text{Fe}$  and  $^{59}\text{Co}$ . Data were taken from Ref. [27].

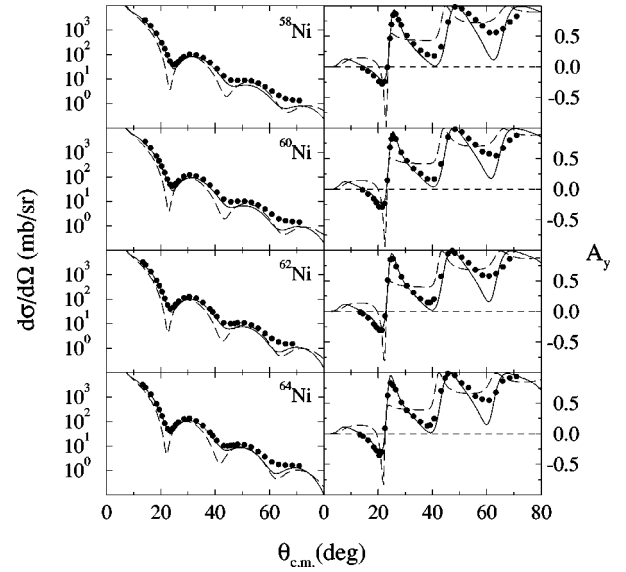


FIG. 8. As for Fig. 1 but for  $^{58,60,62,64}\text{Ni}$ . Data were taken from Ref. [27].

did in our 200 MeV analysis [4]. Nevertheless, in every case, the results obtained in the  $g$ -folding model are in much better agreement overall with the data, especially with the analyzing powers, with the level of agreement being actually quite good.

The trends in magnitudes and shape of the data with mass remain and are enhanced with this set of nuclei. Notably the first minimum of the cross section becomes more pronounced as does the first minimum in the analyzing power.

### C. Heavy nuclei ( $A > 64$ )

For nuclei with mass in excess of 70, shell model calculations, even in restricted spaces, generally are not feasible. The increase in the number of valence nucleons and an increase in the number of SP states that may be occupied cause the dimension of the model space to become prohibitively large. Therefore, we have chosen a simple packing model to specify the OBDME's. In that model, nuclear shells are filled in sequence from the lowest lying shells to the Fermi level. As the results of our calculations are not particularly sensitive to the diffuseness in the nuclear density in this mass region, this is not a bad approximation. A more important feature is the choice of the oscillator length for the single-nucleon bound-state functions. Again, we have chosen  $b = A^{1/6}$  fm for all shells. A more reasonable approach would be to assume a different oscillator parameter for the protons and neutrons. By that means, the proton and neutron total distributions could be kept similar despite the neutron excesses.

The results for the scattering from  $^{89}\text{Y}$ ,  $^{90}\text{Zr}$ , and  $^{98,100}\text{Mo}$  are displayed in Fig. 9. For the four cases presented, the cross-section data are well reproduced by our  $g$ -folding model predictions to  $50^\circ$ . Thereafter, our results slightly underestimate the data in the region of the minimum at  $\sim 55^\circ$ . While the  $t$ -folding model results give similar shapes for the cross sections, the second minimum at  $35^\circ$  is an order of magnitude deeper than that observed and also as predicted by the  $g$ -folding model result. The differences between the two



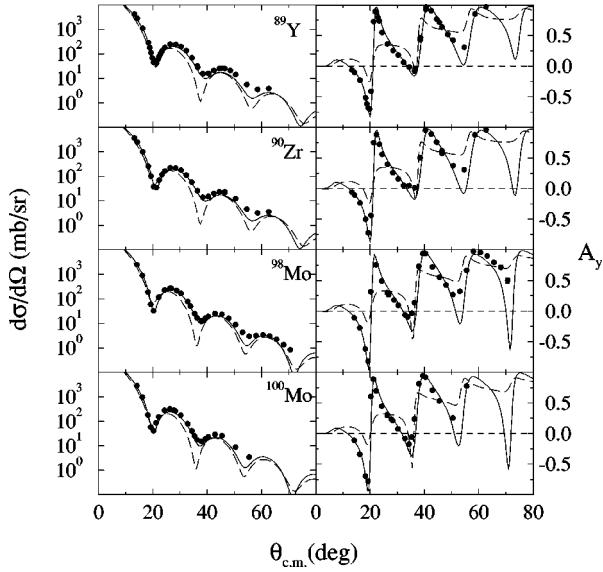


FIG. 9. As for Fig. 1 but for  $^{89}\text{Y}$ ,  $^{90}\text{Zr}$ , and  $^{98,100}\text{Mo}$ . Data were taken from Ref. [27].

models are far more striking in the comparisons of the analyzing powers. The  $g$ -folding results are in very good agreement with the data to  $50^\circ$ . The results obtained with the  $t$ -folding model definitely are not. The latter do not reproduce the shape or the magnitude of the data. It is interesting to note that the region in which the analyzing power is underestimated by the  $g$ -folding results is also that in which the cross section is underestimated. Since the analyzing power is scaled by the cross section, an improvement in the level of agreement in the cross section in this region may also produce an improvement in the analyzing power.

Our  $g$ -folding model results are compared with data for the scattering of 65 MeV protons from  $^{118}\text{Sn}$  and  $^{144,152,154}\text{Sm}$  in Fig. 10. For these cases, the first two minima in the cross-section data are very well reproduced by the  $g$ -folding model results as is the third minimum in the

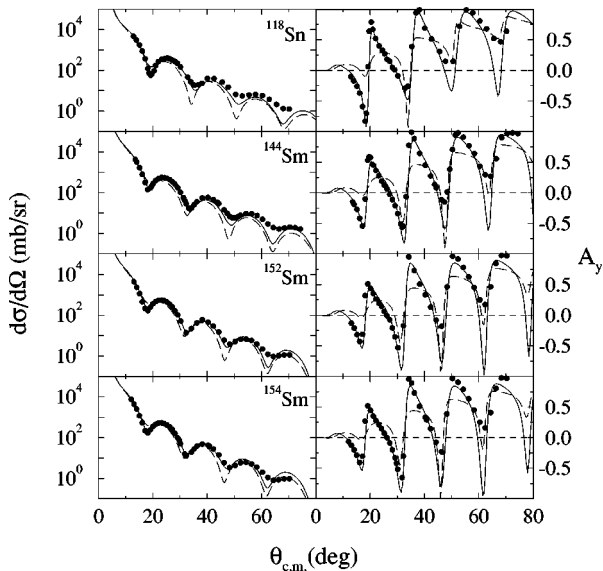


FIG. 10. As for Fig. 1 but for  $^{118}\text{Sn}$  and  $^{144,152,154}\text{Sm}$ . Data were taken from Refs. [25,27,29].

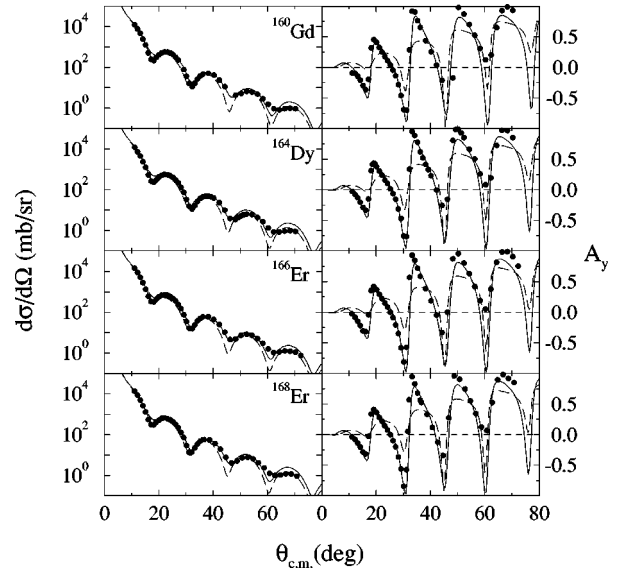


FIG. 11. As for Fig. 1 but for  $^{160}\text{Gd}$ ,  $^{164}\text{Dy}$ , and  $^{166,168}\text{Er}$ . Data were taken from Refs. [29–31].

$^{152,154}\text{Sm}$  data. The same level of agreement is achieved in the analyzing powers between the data and results from the  $g$ -folding calculations. The same dramatic difference between the  $g$ - and  $t$ -folding models is observed in the analyzing power as was the case with the results in the mass-90 region.

We show comparisons of our model predictions with data for the scattering from nuclei ranging between  $^{160}\text{Gd}$  and  $^{180}\text{Hf}$  in Figs. 11 and 12. The level of agreement in the cross section between the data and the  $g$ -folding model results is again very high. The results obtained using the  $t$ -folding model have a tendency to underestimate the data, especially at the minima above  $40^\circ$ , and do not predict the locations of those minima. Nevertheless, the shape of the cross-section data generally is reproduced. Those levels of agreement are not reflected in the comparisons of analyzing powers. The

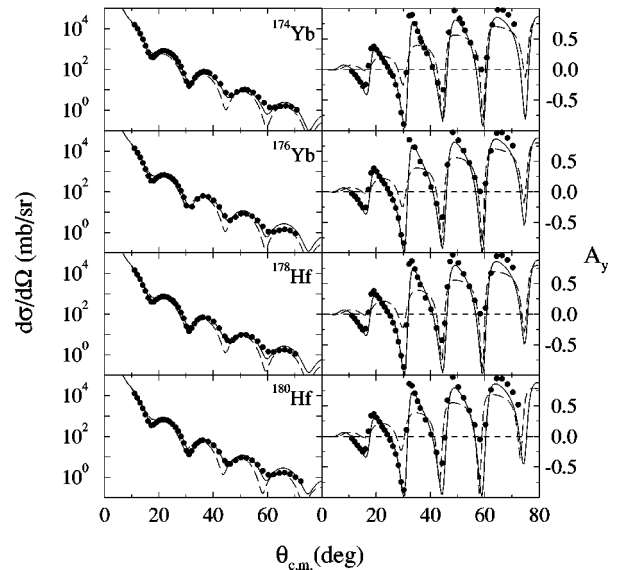


FIG. 12. As for Fig. 1 but for  $^{174,176}\text{Yb}$  and  $^{178,180}\text{Hf}$ . Data were taken from Refs. [31,32].

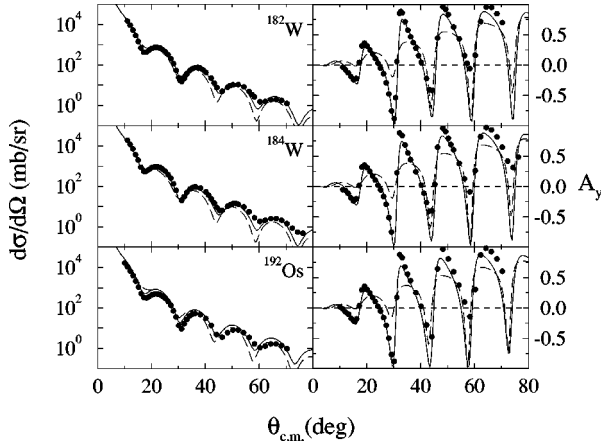


FIG. 13. As for Fig. 1 but for  $^{182,184}\text{W}$  and  $^{192}\text{Os}$ . Data were taken from Refs. [30,32].

$g$ -folding model predictions are results that generally reflect the data, although there might be some suggestion from the comparisons with the low angle data that larger oscillator lengths are preferable. The  $t$ -folding model ones reproduce neither the magnitudes nor the shapes of the data.

The data for the scattering from  $^{182,184}\text{W}$  and  $^{192}\text{Os}$  are compared with our  $g$ - and  $t$ -folding model predictions in Fig. 13. The level of agreement with the cross-section and analyzing power data for the scattering from the W isotopes is as observed for the cases discussed already. The results for the scattering from  $^{192}\text{Os}$  are a little perplexing. The data suggest a somewhat weaker cross section than those for the elastic scattering from neighboring nuclei. Yet the shape and magnitude of the analyzing power is similar. Our  $g$ -folding results overestimate the cross section by 60–70% at low scattering angles.

We compare the results of our microscopic optical model calculations with the data for scattering from nuclei with  $A > 200$  in Fig. 14. All the data, for both the cross section and analyzing power, show similar structure, with which our  $g$ -folding model results agree well in both shape and magni-

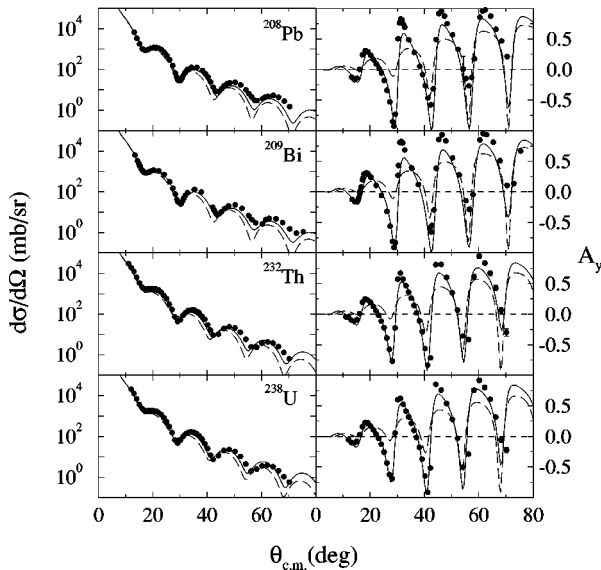


FIG. 14. As for Fig. 1 but for  $^{208}\text{Pb}$ ,  $^{209}\text{Bi}$ ,  $^{232}\text{Th}$ , and  $^{238}\text{U}$ . Data were taken from Refs. [27,33].

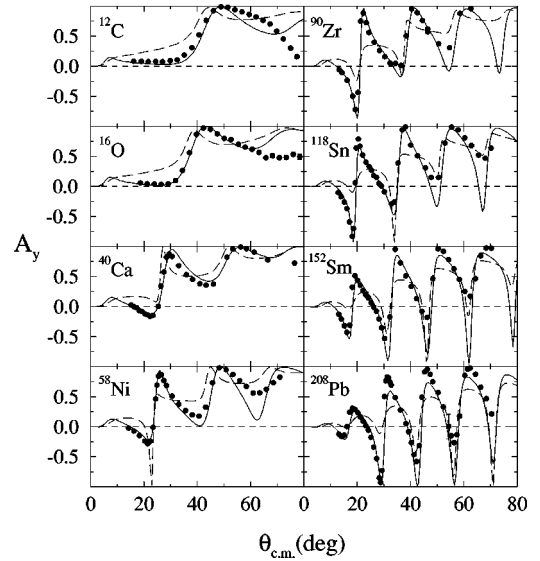


FIG. 15. The analyzing power  $A_y$  from the elastic scattering of 65 MeV protons from  $^{12}\text{C}$ ,  $^{16}\text{O}$ ,  $^{40}\text{Ca}$ ,  $^{58}\text{Ni}$ ,  $^{90}\text{Zr}$ ,  $^{118}\text{Sn}$ ,  $^{152}\text{Sm}$ , and  $^{208}\text{Pb}$ . The data (dots) are compared with the results of our microscopic model calculations for the cases when medium effects are included (solid curves) or are ignored (dashed curves). Data were taken from Refs. [25–27,29].

tude. However, the slight differences in the positions of the minima between the cross-section data and our predictions suggest that the choice of oscillator wave functions is less than optimal. Yet the comparison with the analyzing power data is remarkably good in tracking the shape and positions of the minima. It is clear once more that the effects of the nuclear medium in defining the effective  $NA$  optical potential are quite important. While the  $t$ -folding model results track the positions of the maxima and minima in the analyzing powers to some extent, they fail to reproduce the observed magnitudes. This is also reflected in the cross sections, where the positions of the minima also are not reproduced.

#### D. Mass dependences of spin observables

In Figs. 15 and 16 we display the analyzing powers and spin rotations ( $R$ ) for the scattering of 65 MeV polarized protons from a set of eight nuclei ranging from  $^{12}\text{C}$  to  $^{208}\text{Pb}$ . The curves represent the same model predictions as given in the preceding figures. One can see from Fig. 15 that the structure of the measured analyzing power changes in a consistent way as the mass of the target increases. Indeed, the depth of the first minimum and the sharp rise between this and the next maximum become more pronounced with target mass to  $^{118}\text{Sn}$ . As the target mass increases, the magnitude of this minimum and of the following maximum is greatly suppressed. The absolute value of those minima and maxima approaches unity for the heaviest nuclei. As noted in the discussions of individual results, the  $g$ -folding calculations predict observed analyzing powers very well and at scattering angles for which the cross-section data (usually of magnitude  $> 1$  mb/sr) also are well reproduced.

There is a limited set of measurements [25] of the spin rotations for the elastic scattering of 65 MeV polarized protons from nuclei. These are displayed in Fig. 16. For the lightest four nuclei presented, the comparison between the

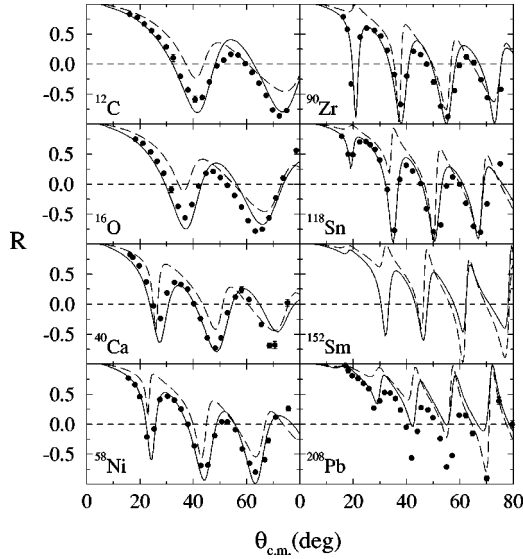


FIG. 16. As for Fig. 15 but for the spin rotation  $R$ . Data were taken from Ref. [25].

$g$ -folding model results and data is quite good. Those results from the  $t$ -folding model calculations do not match observation as adequately. The differences between the  $g$ - and  $t$ -folding models are far more pronounced with the scattering from the heavier targets. While the  $g$ -folding model results again give reasonable agreement with the data, the  $t$ -folding model results fail to reproduce both shapes and magnitudes. Indeed, that model predicts a maximum at  $\sim 20^\circ$  in the spin rotation for the scattering from  $^{90}\text{Zr}$  and  $^{118}\text{Sn}$ ; the data indicate a minimum at that angle and such is predicted by the  $g$ -folding model. While there are no data for the scattering from  $^{152}\text{Sm}$ , that difference between the models is also apparent. Also, by this mass, the first minimum has almost disappeared. In the case of scattering from  $^{208}\text{Pb}$ , the result obtained from the  $g$ -folding model reflects the shape of the data, although it overestimates the observed magnitude above  $30^\circ$ . A possible improvement to this result is to use a different set of SP wave functions, as is discussed below.

**E. Effect of varying the oscillator length**

For the descriptions of the scattering for all nuclei up to and including  $^{20}\text{Ne}$  we have used SP wave functions which have been set by fits to electron scattering data. For heavier targets, SP wave functions of HO form with  $b=A^{1/6}$  fm have been used. In general, this choice has produced very good results in comparison with data, but it is instructive to investigate the sensitivity of our calculations to variations in that choice. For this example, we compare the results of two  $g$ -folding calculations with scattering data from  $^{58}\text{Ni}$  and  $^{208}\text{Pb}$  in Fig. 17. Therein, the solid line shows the results of our calculations made using the standard value, that is, 1.97 fm and 2.43 fm for  $^{58}\text{Ni}$  and  $^{208}\text{Pb}$ , respectively. The dashed lines display the results obtained when the oscillator length was chosen to give a much better fit to the cross-section data. Note that these choices are predicated on the simple structure models assumed for both nuclei. Specific shell effects are expected to have some effect on the predictions of cross sections. The revised parameters are 1.87 fm and 2.35 fm for  $^{58}\text{Ni}$  and  $^{208}\text{Pb}$ , respectively. Those lengths were used for all

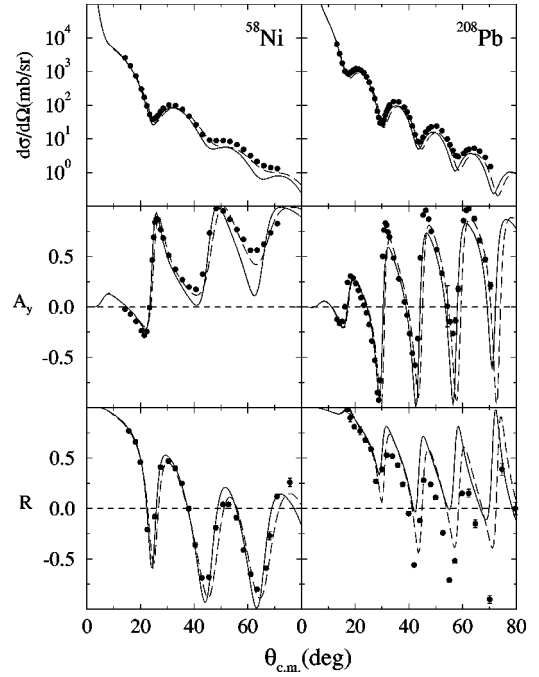


FIG. 17. The differential cross sections (top), analyzing powers (middle), and spin rotation (bottom) from the elastic scattering of 65 MeV protons from  $^{58}\text{Ni}$  and  $^{208}\text{Pb}$ . The data (dots) are compared with the results of our microscopic model calculations when differing oscillator lengths for the bound-state wave functions are used. The solid lines represent the  $b=A^{1/6}$  choice displayed previously (1.97 fm for  $^{58}\text{Ni}$ , 2.43 fm for  $^{208}\text{Pb}$ ), while the dashed curves represent fitted values for  $b$  (1.87 fm for  $^{58}\text{Ni}$ , 2.35 fm for  $^{208}\text{Pb}$ ). Data were taken from Refs. [25,27].

orbits. The improvement in the results with the new SP wave functions is very evident. There is much better agreement between the calculation and experiment for both nuclei, although the position of the minima in the cross section for the scattering from  $^{58}\text{Ni}$  is greater than observation. Using these new sets of wave functions, one observes now much better agreement with the data for both spin observables. In the case of  $^{208}\text{Pb}$ , the significant improvement in the spin rotation has been achieved with only a 3% decrease in the oscillator length.

**IV. CONCLUSIONS**

Optical potentials for the elastic scattering of 65 MeV protons from nuclei have been obtained by folding medium-dependent effective  $NN$  interactions with a specification of the ground state for each nucleus, and also with SP wave functions of either WS or HO form. Those optical potentials are complex and nonlocal and the scattering phase shifts and  $S$  matrices, from which predictions of the measured quantities were obtained, result by solving the relevant nonlocal Schrödinger equations.

We have obtained good to excellent agreement with scattering data from targets ranging from  $^6\text{Li}$  to  $^{238}\text{U}$  using the optical potentials so defined. The framework by which the results were obtained is entirely parameter free; no adjustment of any part of the input was necessary. Thus the non-relativistic mean-field theory for  $pA$  scattering based upon the infinite matter  $g$  matrices is reliable for proton energies down to 65 MeV. This gives encouragement for these tech-

niques to be used in analyses of data from radioactive beam experiments. As the optical potentials are derived directly from the nucleon distributions, instead of averaged charge or matter distributions, this would provide detailed information on the structures of exotic nuclei, as was the case in the study of  ${}^6,8\text{He}$  [7] and of  ${}^9,11\text{Li}$  [8].

## ACKNOWLEDGMENTS

This research was supported by a research grant from the Australian Research Council. We would like to thank Prof. H. Sakaguchi for providing tabulations of much of the data we display herein.

- 
- [1] P. J. Dortmans and K. Amos, *Phys. Rev. C* **49**, 1309 (1994).  
 [2] S. Karataglidis, P. J. Dortmans, K. Amos, and R. de Swiniarski, *Phys. Rev. C* **52**, 861 (1995).  
 [3] L. Rikus, K. Nakano, and H. V. von Geramb, *Nucl. Phys.* **A414**, 413 (1984).  
 [4] P. J. Dortmans, K. Amos, and S. Karataglidis, *J. Phys. G* **23**, 183 (1997).  
 [5] P. J. Dortmans, S. Karataglidis, K. Amos, and R. de Swiniarski, *Phys. Rev. C* **52**, 3224 (1995).  
 [6] P. J. Dortmans, K. Amos, and S. Karataglidis, *Phys. Rev. C* **55**, 2723 (1997).  
 [7] P. J. Dortmans, K. Amos, and S. Karataglidis, in *Proceedings of the 8th International Conference on Nuclear Reaction Mechanisms*, edited by E. Gadioli (Università degli Studi di Milano, Milano, 1997), p. 13.  
 [8] S. Karataglidis, P. G. Hansen, B. A. Brown, K. Amos, and P. J. Dortmans, *Phys. Rev. Lett.* **79**, 1447 (1997).  
 [9] P. J. Dortmans, K. Amos, and S. Karataglidis, *Phys. Rev. C* **57**, 2433 (1998).  
 [10] Ch. Elster and P. C. Tandy, *Phys. Rev. C* **40**, 881 (1989); Ch. Elster, T. Cheon, E. F. Redish, and P. C. Tandy, *ibid.* **41**, 814 (1990); H. F. Arellano, F. A. Brieva, and W. G. Love, *ibid.* **41**, 2188 (1990); **42**, 1782 (1990); **43**, 2734 (1991); **50**, 2480 (1994), and references cited therein.  
 [11] H. F. Arellano, F. A. Brieva, and W. G. Love, *Phys. Rev. C* **52**, 301 (1995).  
 [12] H. F. Arellano, F. A. Brieva, M. Sander, and H. V. von Geramb, *Phys. Rev. C* **54**, 2570 (1996).  
 [13] Ch. Elster and S. P. Weppner, *Phys. Rev. C* **57**, 189 (1998).  
 [14] D. C. Zheng, B. R. Barrett, J. P. Vary, W. C. Haxton, and C.-L. Song, *Phys. Rev. C* **52**, 2488 (1995).  
 [15] J. Raynal, computer code DWBA91, Report No. NEA1209/02, 1991.  
 [16] S. Karataglidis, B. A. Brown, K. Amos, and P. J. Dortmans, *Phys. Rev. C* **55**, 2826 (1997).  
 [17] M. I. Haftel and F. Tabakin, *Nucl. Phys.* **A158**, 1 (1970).  
 [18] P. J. Dortmans and K. Amos, *J. Phys. G* **17**, 901 (1991).  
 [19] M. Lacombe, B. Loiseau, J. M. Richard, R. Vinh Mau, J. Côté, P. Pireès, and R. de Tourreil, *Phys. Rev. C* **21**, 861 (1980).  
 [20] J. Raynal, "Aspects Geometriques des Reactions," Saclay Report No. CEA-N-1529, 1972.  
 [21] C. W. De Jager, H. De Vries, and C. De Vries, *At. Data Nucl. Data Tables* **14**, 479 (1974); H. De Vries, C. W. De Jager, and C. De Vries, *ibid.* **36**, 495 (1987); G. R. Satchler, *Nucl. Phys.* **A579**, 241 (1994).  
 [22] M. Tosaki, M. Fujiwara, K. Hosono, T. Noro, H. Ito, T. Yamazaki, H. Ikegami, and M. Kamimura, RCNP Annual Report, 1985 (unpublished), p. 21.  
 [23] C.-B. Moon *et al.*, *Phys. Lett. B* **297**, 39 (1992).  
 [24] S. Kuwamoto, M. Nakamura, T. Nakano, H. Kaneko, H. Akimune, S. Sawada, S. Yamamura, and S. Kobayashi, RCNP Annual Report, 1990 (unpublished), p. 6.  
 [25] M. Yosoi *et al.*, RCNP Annual Report, 1985 (unpublished), p. 4.  
 [26] S. Kato *et al.*, *Phys. Rev. C* **31**, 1616 (1985).  
 [27] H. Sakaguchi, M. Nakamura, K. Hatanaka, A. Goto, T. Noro, F. Ohtani, H. Sakamoto, H. Ogawa, and S. Kobayashi, *Phys. Rev. C* **26**, 944 (1982); H. Sakaguchi, in "Memoirs of the Faculty of Science," Kyoto University Series A of Physics **36**, 305 (1983).  
 [28] T. Noro, H. Sakaguchi, M. Nakamura, K. Hatanaka, F. Ohtani, H. Sakamoto, and S. Kobayashi, *Nucl. Phys.* **A366**, 189 (1981).  
 [29] F. Ohtani, H. Sakaguchi, M. Nakamura, T. Noro, H. Sakamoto, H. Ogawa, T. Ichihara, M. Yosoi, and S. Kobayashi, *Phys. Rev. C* **28**, 120 (1983); H. Sakaguchi (private communication).  
 [30] T. Ichihara, H. Sakaguchi, M. Nakamura, M. Yosoi, M. Ieiri, Y. Takeuchi, H. Togawa, T. Tsutsumi, and S. Kobayashi, *Phys. Rev. C* **36**, 1754 (1987); H. Sakaguchi (private communication).  
 [31] T. Ichihara *et al.*, *Phys. Rev. C* **29**, 1228 (1984); H. Sakaguchi (private communication).  
 [32] H. Ogawa *et al.*, *Phys. Rev. C* **33**, 834 (1986); H. Sakaguchi (private communication).  
 [33] Y. Takeuchi, H. Sakaguchi, M. Nakamura, T. Ichihara, M. Yosio, M. Ieiri, and S. Kobayashi, *Phys. Rev. C* **34**, 493 (1986); H. Sakaguchi (private communication).  
 [34] S. Karataglidis, P. J. Dortmans, and K. Amos, "Comment on 'Energy dependence of the  $NN$   $t$  matrix in the optical potential for elastic nucleon-nucleus scattering,'" University of Melbourne Report No. UM-P-98/03, 1998, *Phys. Rev. C* (submitted).  
 [35] G. Roy *et al.*, *Nucl. Phys.* **A442**, 686 (1985); J. J. Kelly, *Phys. Rev. C* **38**, 1490 (1988).